JACS Au
AN OPEN ACCESS JOURNAL OF THE AMERICAN CHEMICAL SOCIETY

pubs.acs.org/jacsau
Article

Antidiabetic Close Loop Based on Wearable DNA−Hydrogel Glucometer and Implantable Optogenetic Cells

Tiantian Man, Guiling Yu, Fulin Zhu, Yaqi Huang, Yueyu Wang, Yan Su, Shengyuan Deng,* Hao Pei, Li Li, Haifeng Ye,* and Ying Wan*

Cite This: *JACS Au* 2024, 4, 1500−1508
Read Online

ABSTRACT: Diabetes mellitus and its associated secondary complications have become a pressing global healthcare issue. The current integrated theranostic plan involves a glucometer-tandem pump. However, external condition-responsive insulin delivery systems utilizing rigid glucose sensors pose challenges in on-demand, long-term insulin administration. To overcome these challenges, we present a novel model of antidiabetic management based on printable metallo-nucleotide hydrogels and optogenetic engineering. The conductive hydrogels were self-assembled by bioorthogonal chemistry using oligonucleotides, carbon nanotubes, and glucose oxidase, enabling continuous glucose monitoring in a broad range (0.5−40 mM). The optogenetically engineered cells were enabled glucose regulation in type I diabetic mice via a far-red light-induced transgenic expression of insulin with a month-long avidity. Combining with a microchip-integrated microneedle patch, a prototyped close-loop system was constructed. The glucose levels detected by the sensor were received and converted by a wireless controller to modulate far-infrared light, thereby achieving on-demand insulin expression for several weeks. This study sheds new light on developing next-generation diagnostic and therapy systems for personalized and digitalized precision medicine.

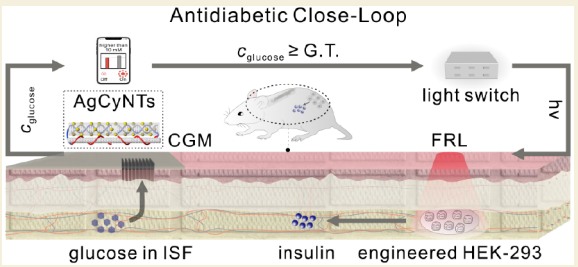

KEYWORDS: *diabetes mellitus, conductive DNA hydrogel, continuous glucose monitoring, hollowed microneedle array chip, optogenetic metabolism circuitry*

INTRODUCTION

Diabetes is a severe chronic disease that annually affects the lives of almost 425 million people worldwide.[1,2] The current treatment plans generally adopt exogenous insulin supplementation to regain glycemic homeostasis for insulin-deficient type I diabetic (T1D) patients.[3,4] Although periodical subcutaneous injection is the gold standard, the intrinsic invasiveness of the method and the associated discomfort to the user have evoked the ongoing quest for more gentle solutions as alternatives to daily administration.[5−10] One such viable option is the microneedle array patch, which allows self-regulated transdermal insulin delivery and facilitates *in situ* insulin release via glucose-responsive swelling, shrinking, or degradation of stuffed polymeric pillars.[6−8] Nonetheless, unchecked seepage and loss of activity of the impregnated affinity elements (*e.g.*, glucose oxidase (GOx), phenylboronic acid, *etc.*) affect the dose precision of such devices.[6−8,10] In addition, drawbacks like limited insulin-loading capacity and common biosafety concerns related to microfabrication can be problematic for clinical usage.[11,12] Hence, it remains challenging for these systems to provide an on-demand, long-term insulin administration in patients with diabetes mellitus. According to the principle of diabetes management, programmable and sustainable management with minimal intervention is desirable. However, the development of such systems is still in its infancy.

Precise glycemic control in real time requires an integrated theranostic plan involving a glucometer-tandem insulin pump, wherein data transfer occurs from the assay terminal to the insulin dispenser.[5−7] The plan needs to fulfill the following requirements: (1) real-time tracking of the glucose levels to provide timely feedback on insulin release. The current wearable sensing devices, whether in rigid planar film forms or adhesive metallo-needle punctures,[5,9,10] cannot dwell long on the torso skin, which results in poor glucose regulation. (2) On-demand release of insulin for effective blood glucose regulation. Currently, insulin reservoirs that rely on stimulus response for controlled release often exhibit slow response times or insufficient flow, resulting in treatment failure.[5,9] (3) Connection between the two main modules. Imprecise stimulus-responsive strategy may lead to premature or delayed

Received: January 9, 2024
Revised: March 23, 2024
Accepted: March 25, 2024
Published: April 6, 2024

https://doi.org/10.1021/jacsau.4c00033
JACS Au 2024, 4, 1500−1508

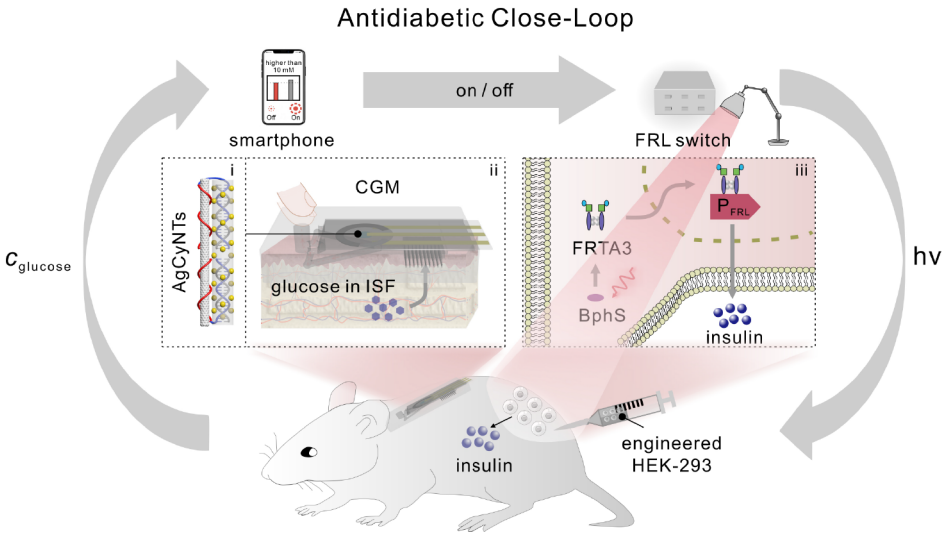

Figure 1. Schematic illustration of the conceived antidiabetic closed-loop system. It comprises a customized continuous glucose monitor (CGM) for on-body glycemia tracing, a smartphone-controlled light switch, and optogenetic cells responsive to FRL. These critical components cooperated to enable endogenous insulin regulation in a type I diabetes mouse model. Inset (i): hybrid DNA hydrogel serving as the conductive scaffold; (ii) microchip-integrated microneedle patch functioning as an ISF sampler activated by finger pressure; (iii) introduction of light-responsive signaling in engineered HEK-293 cells—FRL stimulation of the photoreceptor BphS triggers the binding of FRTA3 to the chimeric promoter PFRL, facilitating insulin secretion.

insulin release, thereby resulting in hypoglycemia or hyperglycemia.[9]

To achieve precise spatiotemporal release of insulin, a new therapeutic mode for diabetes was developed based on the cutting-edge technologies of microchip-integrated microneedle patch and optogenetics (Figure 1). The glucose sensor in the patch was molded out of conductive hydrogels, namely AgCyNTs, with metallo-nucleotide formulation of Ag^+-conjugated polycytosine-grafted carbon nanotubes, orthogonal bonding between cytidine borate diesters and cytosines (i). This hybridization of metallo-nucleotide with carbon nanotubes resulted in a redox-active soft substrate with excellent elasticity and malleability, capable of carrying a large payload of GOx. The microchip-integrated microneedle patch facilitated the ease of finger-actuated sample collection from interstitial fluids (ISF) (ii).[13,14] Inspired by our previous work on light-inducible transgene expression circuitry,[15,16] we further engineered type I diabetic (T1D) mice with HEK-293 cells secreting insulin under far-red-light (FRL) (iii). A contactless and rhythmic insulin control loop can be formed linking the model animal, glycemia detector, mobile App console, and optic shutter without the need for external maintenance. Moreover, by patching all of the miniaturized hardware in a Bluetooth grid and setting up specified glycemic thresholds, a semiautonomous illumination system that can operate for weeks is established. The closed-loop design involving a continuous glucose monitoring and an optogenetically controlled insulin release system may offer significant benefits for the treatment of Type I diabetes in the future.[15]

RESULTS AND DISCUSSION

Fabrication and Characterization of Metallo-Nucleotide Hydrogel

Electrons could shuttle through DNA over distances of tens of nanometers;[17−19] however, unmodified DNA strands lack sufficient electrical conductance for such nanoelectronic application. Exchanging some Watson−Crick base pairs by metal complexes in DNA favors charge transport.[19] Inspired by this, we constructed the metallo-nucleotide hydrogels, where complexes mediated by cations formed between natural nucleobases and nucleosides.[20,21] As described in Figure 2a, cytidine-borate diester is initially formed *via* the addition of $B(OH)_3$ and cytidine (i).[20,21] Subsequently, it was integrated with diblock single-stranded DNA (termed $(GT)_{20}$·C_{15})-modified single-walled carbon nanotubes (NTs); the NTs were selected as the model owing to their excellent conductivity and outstanding mechanical strength. Specifically, $(GT)_{20}$ was incorporated to improve the water solubility of NTs, while C_{15} for cross-linking with cytidine.[22,23] Together, hybrid interactions coordinated by Ag^+ occurred between the two building blocks (ii). The conductive hydrogels included (1) Ag^+-intercalated cytidine dimerization, (2) Ag^+-fastened interfacial H-bonding among cytidines and cytosines, and (3) Ag^+-stabilized NTs modified with $(GT)_{20}$·C_{15}. These three primary metallo-nucleosides facilitated the formation of a composited hydrogel, consisting of an interconnected fibrous structure of AgCyNTs. After cross-linking, UV light was applied to the hydrogels converting excessive Ag^+ into silver nanoparticles (AgNPs) on site (iii).[24,25] Atomic force microscopic (AFM) topographies (Figure S1) and inset cross-sectional profiles revealed that pristine NTs (a) thicken after hydrogel formation (b) in the presence of Ag^+. Energy-dispersive X-ray (EDX) elemental mapping unveiled the presence of a dense population of AgNPs (Figure S2, right).

To gain a deeper understanding of the observed hydrogelation, we explored the influence of Ag^+ by introducing cysteine. As displayed in Figure S3, the ensemble can reversibly switch between the gel and sol states by the cyclic addition of Ag^+ and cysteine. Moreover, the viscosity exhibited fluctuations within the range of $10-10^3$ Pa as Ag^+ ions were detached through thiol complexation and subsequently complemented,[26,27] leading to transitions between a liquified and solidified phase (Figure S4). The latter could only be reformed upon the $AgNO_3$ refilling, which signified the contribution of

https://doi.org/10.1021/jacsau.4c00033
JACS Au 2024, 4, 1500−1508

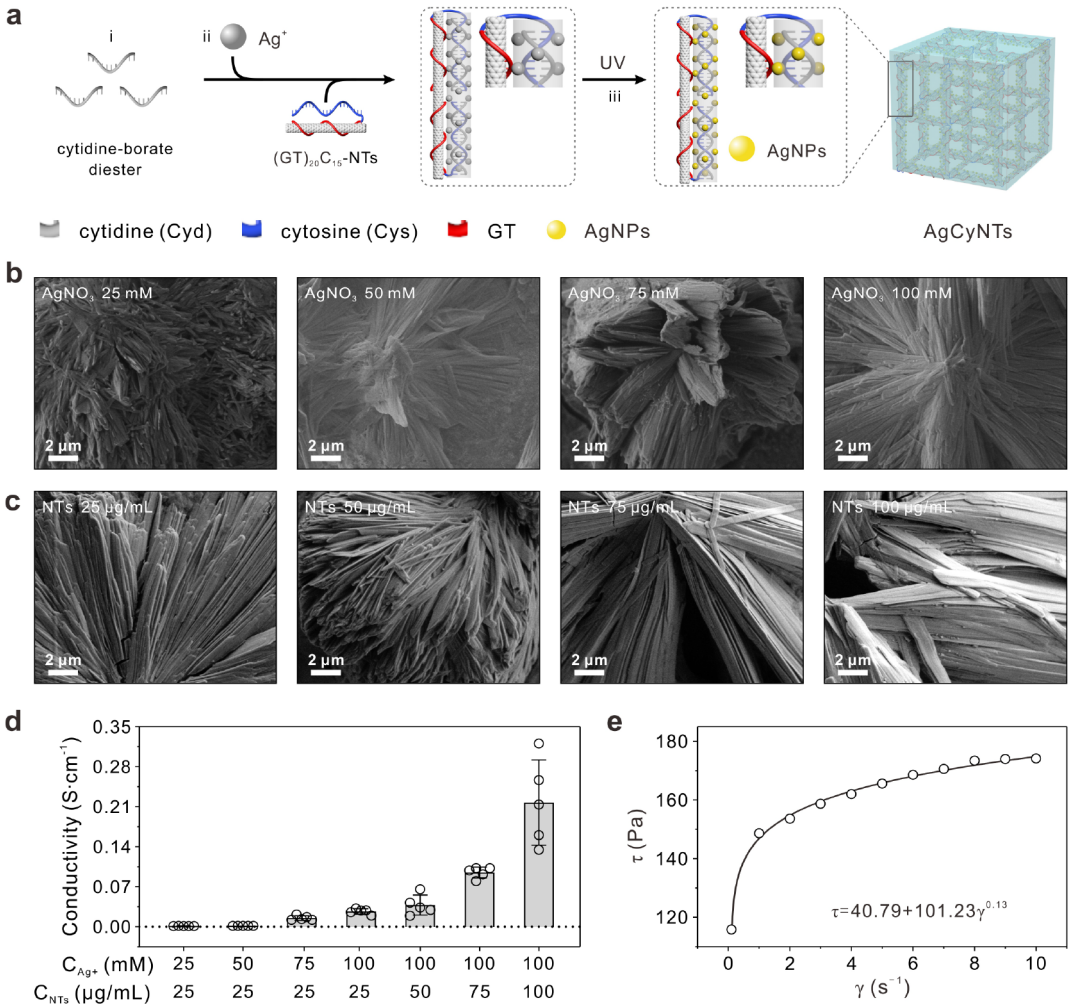

Figure 2. (a) Preparation of AgCyNTs involves a stepwise procedure from left to right: (i) borate affinity with cytidine; (ii) its intermingling with ssDNA-pendant NT that studded with Ag^+; (iii) 365 nm light-assisted deposition of AgNPs on the scaffold. The panel below shows SEM images of AgCyNTs prepared with varying amounts of (b) $AgNO_3$ (20, 50, 75, and 100 mM) plus 100 μg/mL NTs, and (c) NTs (25, 50, 75, and 100 μg/mL) plus 100 mM $AgNO_3$. (d) Conductivity of AgCyNTs at different molar fractions of Ag^+ and NTs. (e) Shearing stress (τ) plotted against shear rate (γ) for AgCyNTs (100 mM Ag^+, 100 μg/mL NTs) fitted to the Herschel–Bulkley model: $\tau = \tau_0 + K\gamma^n$, where τ_0 denotes the yield tension, K represents the consistency index, and n means the flow behavior.

this cation to the cohesion of AgCyNTs. Further investigations into the effects of Ag^+/NTs on the geometric, electrical, and rheological properties revealed as following. First, increasing the content of Ag^+ contributed to overall fibrosis (Figures 2b and S5), whereas the accruement of NTs allowed a longitudinal arrangement (Figures 2cand S6). Second, the electroconductibility increased from 0.038 to 0.19 S/cm (Figures 2d and S7), which was higher than that of cation-free NT-DNA hydrogels (0.016 S/cm),[28] indicating high-throughput electron transfer similar to that observed in a pipeline-like morphology.[29−32] The conductivity of our hydrogels was comparable to or higher than that of other polymeric hydrogels, such as gellan gum (0.12 S/m),[33] PEDOT−PSS (0.074 S/m),[34] and PAA/PEDOT−PSS (0.06−0.12 S/m).[35] Third, the rheological characteristics were analyzed under a strain sweep in Figure S8. The storage modulus (G', blue dot) rapidly declined when the relative strain increased to ∼5%, and intersected with the loss modulus (G'', red) at 40%; this pattern reflected a gel-to-sol transition.[36] Moreover, the step-strain kinetics shown in Figure S9 revealed the thixotropic behavior of the AgCyNTs hydrogel. The hydrogel maintained a gel-like state at a strain of <0.1%, but collapsed swiftly to quasi-liquids at 100% with a reciprocal relation of G'/G''; when the strain was recovered to 0.1%, both G' and G'' recovered fully. In addition, the hydrogel exhibited a shear thinning behavior. By rheologically testing shearing stress (τ) over a range of shear rate (frequency, γ), the resulting flow curve can be well fitted using the Herschel–Bulkley equation as shown in Figure 2e.[37−39] The flow behavior index of n = 0.13 and the yield tension of τ_0 = 40.79 Pa suggest remarkable shear-thinning behavior and easy mobility at low shear rates, respectively. These results collectively indicate that the hydrogel can enable direct 3D printing using additive manufacturing techniques.

Electrochemistry of the Flexible Glucose Sensor

The unique electroconductibility and malleability of AgCyNTs make them promising building blocks for bioelectronic devices.[40−42] Thus, a straightforward inject-printing mechanism was developed to cast a working area of AgCyNTs on the screen-printed electrode (SPE) while immobilizing glucose oxidase (GOx) (Figure S10, see Methods for details). As displayed in Figure S11, the coexistence of insulating GOx

https://doi.org/10.1021/jacsau.4c00033
JACS Au 2024, 4, 1500−1508

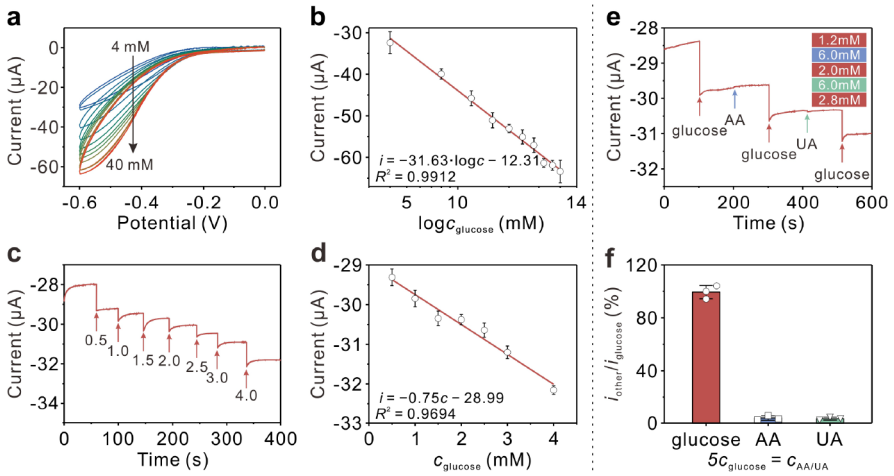

Figure 3. (a) Cyclic voltammogram demonstrates the galvanic response of SPE/AgCyNTs to varying concentrations of glucose ($c_{glucose}$), ranging from 4 to 40 mM. (b) Fitted linear calibration between the gradient of $c_{glucose}$ in (a) (*x*-axis) and the corresponding current at −0.6 V (*y*-axis). (c) Amperometric *i* −*t* titrations with accumulative spiking of given $c_{glucose}$ from 0.5 to 4.0 mM at the arrowed moments. (d) Correlation and the linear fit between the gradient of $c_{glucose}$ in (c) and the potentiostatic current at −0.6 V. (e) Hydrodynamic selectivity tests upon successive supplies of AA and UA (marked by blue and green arrows) in the middle of glucose replenishments (red). Their dosages are scheduled as the inset queue from top to bottom. (f) Normalized steady-state signals of the two interferents (AA and UA at 6 mM) and glucose (1.2 mM). The percentiles are defined by the ratio of the signal intensities of the interferents (i_{other}) to that of glucose ($i_{glucose}$).

within the gel did not significantly affect the redox activity of GOx or the conductivity of the gel. This can be attributed to the effective immobilization of enzyme in the margin of the fiber backbones.[36] Next, in a standard three-electrode configuration (with Ag/AgCl as the reference and glassy carbon as the counter), various glucose concentrations ($c_{glucose}$) were detected through cathodic current changes, resulting from electrocatalytic turnover and the reduction of H_2O_2. The currents at the voltage of interest decreased monotonically as the glucose content increased (Figure 3a), and this result was checked using a nonstop galvanostatic method in the range of [0.5, 4] mM (Figure 3c) with a sensitivity of 0.75 μA/mM (Figure 3d). Beyond 4 mM, another stage of linearity was observed in the segment of [4, 40] mM (3.23 μA/mM; Figure 3b). Over this broad range, the sensor selectively responded to glucose while showing no response to interfering species such as high concentrations of ascorbic acid (AA) and uric acid (UA). As depicted in Figure 3e,f, the response current ratio of interfering chemicals was less than 4.02%. Moreover, the stability analysis revealed that the sensor could maintain its functionality after being stored at 4 °C for up to 20 days, preserving 85.71% of the original response current (Figure S12). Additionally, cyclic voltammetry characterizations demonstrated its exceptional electrochemical stability at 4 °C, with only a marginal decrease of 7.05% observed after 15 repeated scans (Figure S13). Taken together, the excellent sensitivity, selectivity, and stability suggest that AgCyNTs printed glucose sensor has the potential for long-term glucose monitoring.

Optogenetics-Coupled *In Vivo* Insulinotherapy

To achieve a precise correlation between glucose levels and the dosage of insulin release, we next integrated the aforementioned sensing module with the optogenetic therapy module. Traditional continuous glucose monitors (CGMs) employ pointed stainless-steel shafts for the epidermal insertion of sensor tips. In contrast, soft hollow microneedle array (HMNA) chips eliminate the need for bloodletting and compression typically associated with the plunger mechanism.[13,14,43−45] Herein, a miniaturized and portable device powered by mild acupressure was constructed to extract sufficient ISF by channeling from short and extensive HMNA inlets to the biosensing chamber (Figure S14, please refer to specifications in Methods). As depicted in Figure 4a, the device features a lattice arrangement of HMNs on its underside, forming a 10 × 10 matrix (i); each bulge is erected to a height of 700 μm on a base with an inner diameter of approximately 150 μm (ii), (iii). Such a contrivance not only circumvented the siphoning pains but also enhanced the biofluid accessibility, leading to improved consistency in readings. First, the HMNA was adhered to a slice of pigskin, and a (9 × 5) matrix of punctured holes became visible (iv, dashed circles) as expected, highlighting the tissue-penetrating capability of the device.

Subsequently, we enclosed the prototyped CGM circuit with the SPE/metallo-nucleotide hydrogel-housed HMNA as a nodal waypoint. The circuit system contained a potentiostat, a digital-to-analog converter, an analogue-to-digital converter, an *I*/*V*-converter, an amplifier, a wave filter, and a microcontroller unit (Figure 4b). The last one, equipped with a built-in Bluetooth hub, was responsible for signal synchronization with our home-developed mobile application called NJUST-TeleMed. This allowed sharing of the glucose readings ($c_{glucose}$) displayed on the App screen with the microcontroller unit, thus enabling control of the on/off switch on the FRL illuminator. Considering the close correlation between blood glucose concentration and ISF glucose levels,[16,46,47] a glycemic threshold (*i.e.*, GT = 10 mM for T1D mice) was set in the software in advance. When GT > 10 mM, a warning sign would emerge (Figure S15); concurrently, a command would be autodispatched to the physiotherapy lamp (with concomitant notification), activating the *in vivo* insulin biosynthesis to downregulate $c_{glucose}$.

To create a closed-loop system for insulin therapy, an FRL-triggered optogenetic circuit (insulin-expressing engineered cells HEK-$293_{FRL\text{-}SEAP\text{-}P2A\text{-}mINS}$) was constructed based on our previous work.[4] Specifically, the engineered bacterial photo-

https://doi.org/10.1021/jacsau.4c00033
JACS Au 2024, 4, 1500−1508

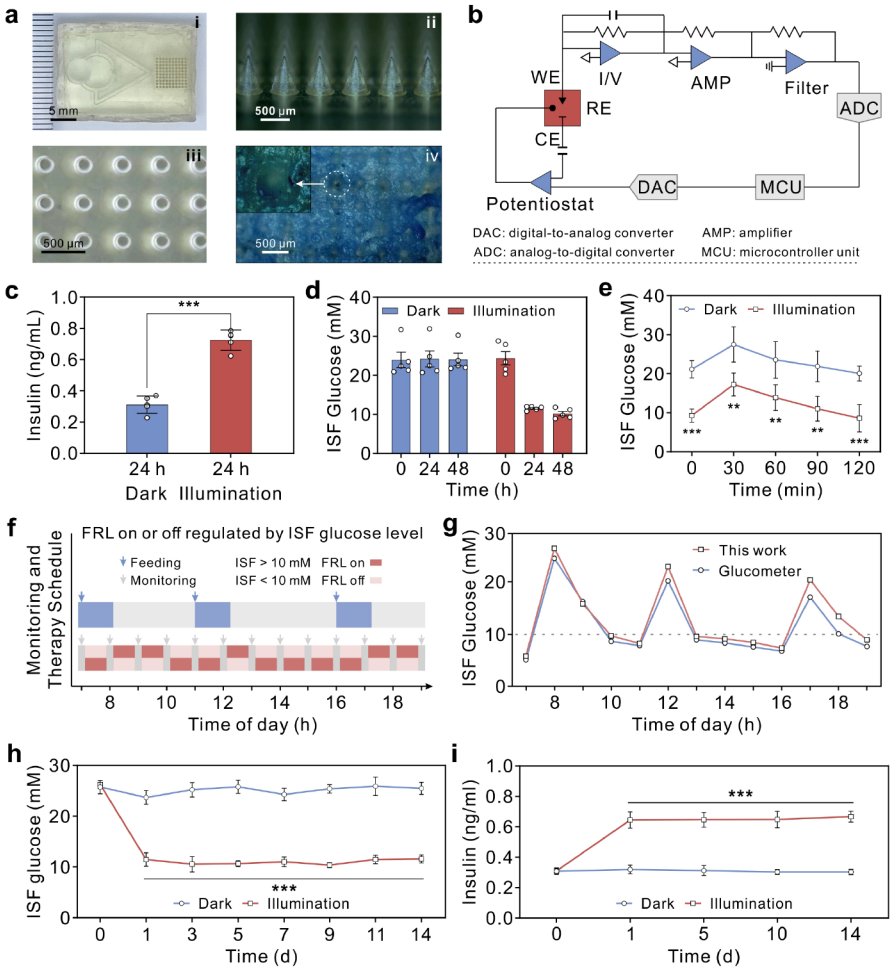

Figure 4. (a) (i) Photograph of an intact microchip-integrated HMNA patch, SEM images of the HMNA from (ii) side and (iii) top views, and (iv) zoom-in image of porcine skin after removal of HMNA. (b) Schematic diagram of the wireless control and transmission system for the CGM, including digital-to-analog converter, amplifier, analog-to-digital converter, and microcontroller unit. Measurement of (c) blood insulin at 24 h and (d) glucose in ISF at 0, 24, and 48 h. Ten T1D mice were intraperitoneally implanted with 2×10^6 transfected HEK-293 cells, with half housed in dark (blue), while the other five exposed to FRL (730 nm, 10 mW/cm^2) for 2 h per day (red). (e) Intraperitoneal glucose tolerance test (IPGTT) at 48 h after implantation with HEK-293 cells. (f) Hourly diagnosis and treatment schedule from 7:00 to 18:00. (g) $c_{glucose}$ in ISF recorded following the schedule in (f) by our devised CGM-patch (red) and a commercialized glucometer (blue). (h) $c_{glucose}$ in ISF at days 1, 3, 5, 7, 9, 11, and 14, and (i) blood insulin at days 1, 5, 10, and 14. Ten T1D mice were intraperitoneally implanted with 2×10^6 transfected HEK-293 cells, with half housed in dark (blue), and the other five were exposed to FRL (730 nm, 10 mW/cm^2) for 2 h per day (red). Data points in (c), (d), and (e) are presented as average ± standard deviation; two-tailed *t* test was calculated for statistics ($n = 5$); $^{**}p < 0.01$, $^{***}p < 0.001$ versus control group (dark).

receptor BphS was activated by 730 nm FRL, converting GTP to c-di-GMP. Increased cytosolic c-di-GMP production triggered FRTA (p65-VP64-BldD) dimerization, which then bound to chimeric promoters PFRL, enabling FRL-triggered secreted human placental alkaline phosphatase (SEAP) and insulin expression. The intracellular c-di-GMP production could be modulated by varying the amount of c-di-GMP-specific phosphodiesterase (YhjH) (Figure S16). We investigated the induction of protein secretion by conducting *in vitro* experiments using HEK-293 cells under FRL irradiation. The long-term stability of SEAP production was first assessed, revealing sustained secretion for up to 14 days upon FRL (Figure S17a). Furthermore, the kinetics of cell secretion were also observed to be dependent on both the intensity and duration of the FRL exposure (Figure S17b,c). Notably, the HEK-293 cells exhibited light-dependent protein secretion dynamics (Figure S17d).

The bioelectronic system was implemented in insulin-deficient T1D mice. The mice were inoculated in advance with the genetically modified HEK-293 cells responsive to FRL and attached with a transdermal HMNA patch, where the patch served as an ISF sampler and a sensor chamber. The changes of $c_{glucose}$ in ISF of each mouse were monitored over a day period and promptly uploaded to App. As mentioned above, the deformable cuvette in the upper layer of HMNA facilitated the migration of the ISF to the enzyme sensor. In the event of a hyperglycemia alert on the phone, the FRL would be activated online to stimulate the production of insulin in T1D mice. As displayed in Figure 4c, the T1D mice that underwent phototherapy demonstrated a restoration of their endogenous insulin levels. Upon extending the measurement for up to 2 days, the diabetic group was able to restore a balance in glucose levels, unlike the control group (Figure 4d). This observation indicated the successful achievement of self-sufficient insulin production. In addition, T1D mice implanted

https://doi.org/10.1021/jacsau.4c00033
JACS Au 2024, 4, 1500−1508

with HEK-293 cells showed improved glucose tolerance (Figures 4e and S18).

Finally, the ability of kinetic maintenance of euglycemia was inspected along the timeline of fixed daily meals: breakfast (7:00 to 8:00), lunch (12:00 to 13:00), and supper (17:00 to 18:00). The intraday postprandial $c_{glucose}$ in the ISF of the T1D mice implanted with HEK-293 cells was evaluated hourly with the glycemic control system (Figure 4f). The FRL was intermittently activated according to the preset GT to prevent hypoglycemia resulting from potential insulin overexpression.[48] The real-time quantitation profile exhibited by our CGM was comparable to those obtained using commercial benchtop equipment in clinics (Figure 4g, Accu-Chek Performa, Roche). Additionally, we investigated the long-term effectiveness of our closed-loop insulin therapy system in diabetic treatment by evaluating the blood insulin levels and ISF glucose in the T1D model mice over multiple days. Notably, the glucose levels were measured after 2 h of daily FRL stimulation to enhance insulin expression in the T1D mice. As depicted in Figure 4h, the illumination group achieved glucose homeostasis unlike the dark control mice after exposure to FRL. Furthermore, FRL led to a significant increase in the insulin levels of the T1D mice compared to those of the dark control mice (Figure 4i). Collectively, an effective closed-loop antidiabetic strategy has been developed.

CONCLUSIONS

In this study, we developed an innovative wearable CGM based on injectable DNA hydrogels in HMNA and microfluidics. To exploit downstream applications, a continuous glucose sensor and an optogenetic circuit were integrated to form a closed-loop antidiabetic system. Such a combination featured (1) the coassembly of metallo-nucleotide(s) and NTs resulted in a fiber-structured DNA hydrogel with not only superior conductivity[49,50] but also distinct viscoelasticity[36] compared to hard bulky electrode materials; (2) the weakly invasive ISF multisampling provided accurate profiling of the glycemic levels; (3) FRL-triggered transcription/translation was superior to the conventional *in vitro* fortification method in terms of self-sustainability; (4) a sentineling server facilitated the relay of CGM output to a microcontroller unit, enabling precise expression of insulin through remote directives. By manipulating the signal pathway through optogenetics, we could effectively control the expression of specific proteins, thereby expanding the possibilities for treating T1D patients. By aligning with emerging data-driven bioelectronic peripherals, we envision that this genetic engineering modification mechanism will be a promising alternative to personalized precision medicine for chronic diseases.[51−54]

METHODS

Functionalization of NTs with Diblock ssDNA

To prepare the $(GT)_{20}C_{15}$-tethered NTs, 1 mg of NTs was dissolved in a 1 mL 2× SSC buffer containing 500 μM $(GT)_{20}C_{15}$.[23] The suspension was subjected to 2 h of sonication (power level: 3 W) in an ice−water bath and subsequently divided into 100-μL aliquots and centrifuged at 17,000 g for 90 min. After the precipitates were decanted, the supernatant was collected and desalinated through three-round ultrafiltration at 6500 rpm per 5 min.

Preparation of DNA Hydrogel

Taking optimal condition as an example, 40 μL of 500 mM cytidine was mixed with 20 μL of 500 mM $B(OH)_3$, 60 μL of 0.5 M $AgNO_3$, 40 μL of 1 mg/mL $(GT)_{20}C_{15}$NTs, and 800 μL of deionized H_2O. Then, 40 μL of 0.5 M trisodium citrate was blended in thoroughly. The mixture was exposed to 365 nm UV light at a 5 cm distance away for 2 h until the reactants turned purplish, which was a signature of excessive Ag^+ reduction into silver nanoparticles (AgNPs).

Conductivity Calculation

The as-prepared hydrogel was printed as a stripe on a piece of glass slide (2 cm × 2 cm) to stay partially dehydrated, whereby the pellets of eGaIn were dispensed at both the long-side ends to ameliorate contact resistance prior to the film impedance (R, Ω).[31] The formula: $\sigma = L_1/(R \times d \times L_2)$, where L_1 and L_2 (cm) indicate the lengths parallel and perpendicular to the current direction, respectively, and d (cm) denotes the thickness/depth of the membrane overlay, was used to assess the conductance (σ, S/cm).

Construction of Glucose Sensor

The working area of an SPE was gilded by electrodeposition in 3 mg/mL $HAuCl_4$ at −0.2 V for 10 min.[55] Subsequently, 5 μL of 1 μM $polyC_{15}$−SH was pipetted to hold still at 4 °C overnight. Next, the hydrogel (5 μL) was spread above to accept 2 h of UV aging at room temperature. Then, the as-modified part of electrode was added to 10 μL of 1 mg/mL glucose oxidase (GOx, 50 kU/mg, Aladdin) for 1 h. Finally, 3 μL of 0.01% Nafion was added on the surface of the working electrode area and was dried at 4 °C for 1 h.

Design and Fabrication of the Wearable CGM

Adapting from the previous report,[44] the microneedle array was proposed by a microfluidic channel as both ISF conduit and collector, which was sketched in SolidWorks 2020. As delineated in Figure S14, this dual-storey structure with a dimension of [24 mm (l) × 18 mm (w) × 5.57 mm (d)] embeds within its top layer a pressable soft spot (Φ 5 mm, d 3 mm), an outlet (Φ 1 mm), and a sensor chip cassette [15 mm (l) × 6 mm (w) × 0.5 mm (d)]. By pressing with a fingertip, a small portion of ISF would be sucked outward across the designated entry to a bifurcated Y-shaped junction, that proceeded to the compartment of the glucometer and discharged upon the egress. On the bottom layer, 100 micropillars were distributed uniformly over a square of 6.6 × 6.6 mm^2 hollowed out with a central spacing of 600 μm and an altitude of 700 μm (Figure S14c). The maximal outer Φ of the tiny cone was settled at 500 μm, and its inner diameter was 150 μm.

The finger-driven ISF sampler was manufactured separately using the following process: polydimethylsiloxane (PDMS, Sylgard-184, Dow Corning) lithography for the upper floor, whereas 3D-printing (MicroX 115, Xingsheng Tech., Guangzhou) with polyurethane acrylate (PUA, Camic, Wuhan) at a 1-μm resolution in the z-axis for the lower floor. Specifically, a chrome mask of the imprinted microchannel was tailor-made by conformity to the standardized protocol.[56] The PDMS concoction in a 1:10 mass ratio of elastomer to monomer was degassed and poured into the mold for 2-h oven baking at 75 °C to coagulate a block finish, which got laminated off and sealed airtight readily for interfacing with the basement under a PDC-MG oxygen plasma (20 W, 60 s, Mingheng Sci. & Tech., Chengdu). The two parts were dovetailed immediately with the aid of a stereomicroscopic aligner. In case of any open-air breaches, the W-668 photoresist (Weisite) was filled in for cure.

Implantation of Bioengineered Cells in Model Animal

FRL-responsive transgenic HEK-293 cells were encapsulated in poly(L-lysine)alginate beads (~200 cells in 400 μm) by using a B-395 Pro encapsulator (BÜCHI Labortechnik AG, Swiss, vibration frequency: 1300 Hz, 200-μm nozzle, 1.10 kV) via a 25 mL syringe at a flow rate of 450 units.[15]

Next, 10-week-old male mice were grouped in five per cage by body weight, fasted for 16 h, and intraperitoneally infused with streptozotocin (in 200 μL of 1:1 citric acid/sodium citrate) at a ratio of 50 mg/kg for 5 days. The mice with fasting blood-sugar level >16.6 mM 2 weeks after the injection were classified as diabetic. In the next step, the 12-week-old T1D mice were shaved for subcutaneous implants of those formulated capsules (~2 × 10^6

https://doi.org/10.1021/jacsau.4c00033
JACS Au 2024, 4, 1500−1508

cells), which were then either kept in the dark (the control) or exposed to FRL (the subject).

Quantification of ISF Volume Extracted by Soft HMNA Chips

The amount of ISF (V_{ISF}) was quantified after sampling, according to eq 1:

$$V_{ISF} = \frac{W - W_0}{\rho} \quad (1)$$

where W_0 and W are the weights of the soft HMNA chips before and after the insertion into mouse skin, respectively, and ρ is the density of ISF and is assumed to be 1 g/mL.[57] The weight changes (wt %) of the soft HMNA chips were 2.9597/3.0241, 2.9596/3.0285, and 2.9624/3.0397. Therefore, the average V_{ISF} = 70.2 μL. Notably, skin pretreatment with the soft HMNA chips for 5 min prior to the ISF collection resulted in a marked increase in ISF collection, which was associated with increased skin hydration.[58]

Therapeutic Efficacy Estimations by Insulin ELISA and IPGTT

Blood was drawn at the 24th h after the implantation, and clotted at 37 °C for 0.5 h and then at 4 °C for 2 h, from which sera were centrifuged out at 10 min, 5000 rpm.[15] (1) An ELISA kit (Mercodia AB, Cat. No. 10-1247-01, Swiss) was picked to evaluate the physiological levels of insulin. (2) For intraperitoneal glucose tolerance test (IPGTT), mice were fasted for 16 h after 2-day therapy and then administrated with 1 g/kg D-glucose. The time-dependent $c_{glucose}$ in every sample was determined online at 0, 30, 60, 90, and 120 min with the developed CGM. The area under the curve (AUC) for IPGTT was determined by the trapezoidal rule.

Antidiabetic Closed-Loop Modeling

Both the dorsal and abdominal hair of the T1D mice were depilated and gauze-cleaned to avoid dermal contamination.[13] After fasting for 12 h until achieving a stable $c_{glucose}$ around 10 mM, the CGM patch was attached onto the back of the T1D mouse. The process began with 5 min local skin hydration to enrich ISF, during which $c_{glucose}$ were monitored hourly in parallel with a clinically approved glucometer (ACCU-CHEK Performa, Roche, U.S.) during daytime from 7:00 to 19:00. Meals were arranged from 7:00 to 8:00, 12:00 to 13:00, and 17:00 to 18:00. At sampling moment, a 5 s finger press was applied to the designated actuator to induce a capillary influx toward the reservoir. A home-compiled App called "NJUST-TeleMed" (Android) retrieved the signal transmitted from MCU and converted it into $c_{glucose}$. If the number reads beyond the default glycemic checkpoint (*i.e.*, GT = 10 mM), then the FRL bulb is automatically activated for 1 h; otherwise, it remains in the off state.

■ ASSOCIATED CONTENT

Supporting Information

The Supporting Information is available free of charge at https://pubs.acs.org/doi/10.1021/jacsau.4c00033.

SEM and AFM micrographs; pictures; viscosity, resistance, modulus, and step strain measurements; voltammetry; CGM stability; and IPGTT assay (Figures S1−S15); signaling pathway regarding insulin-expression (Figure S16); SEAP production performance under FRL illumination, exposure time-dependent SEAP production, and illumination-dependent SEAP (Figure S17); production AUC analysis of the intraperitoneal glucose tolerance test (Figure S18) (PDF)

■ AUTHOR INFORMATION

Corresponding Authors

Shengyuan Deng − *Key Laboratory of Metabolic Engineering and Biosynthesis Technology of Ministry of Industry and Information Technology, Nanjing University of Science and Technology, Nanjing 210094, China;* orcid.org/0000-0002-6382-0976; Email: sydeng@njust.edu.cn

Haifeng Ye − *Institute of Biomedical Sciences and School of Life Sciences, East China Normal University, Shanghai 200241, China;* orcid.org/0000-0002-5482-8116; Email: hfye@bio.ecnu.edu.cn

Ying Wan − *School of Mechanical Engineering, Nanjing University of Science and Technology, Nanjing 210094, China;* orcid.org/0000-0002-3409-0492; Email: wanying@njust.edu.cn

Authors

Tiantian Man − *School of Mechanical Engineering, Nanjing University of Science and Technology, Nanjing 210094, China*

Guiling Yu − *Institute of Biomedical Sciences and School of Life Sciences, East China Normal University, Shanghai 200241, China*

Fulin Zhu − *School of Mechanical Engineering, Nanjing University of Science and Technology, Nanjing 210094, China*

Yaqi Huang − *School of Mechanical Engineering, Nanjing University of Science and Technology, Nanjing 210094, China*

Yueyu Wang − *School of Mechanical Engineering, Nanjing University of Science and Technology, Nanjing 210094, China*

Yan Su − *School of Mechanical Engineering, Nanjing University of Science and Technology, Nanjing 210094, China*

Hao Pei − *Shanghai Key Laboratory of Green Chemistry and Chemical Processes, School of Chemistry and Molecular Engineering, East China Normal University, Shanghai 200241, China;* orcid.org/0000-0002-6885-6708

Li Li − *Shanghai Key Laboratory of Green Chemistry and Chemical Processes, School of Chemistry and Molecular Engineering, East China Normal University, Shanghai 200241, China;* orcid.org/0000-0001-8494-4997

Complete contact information is available at: https://pubs.acs.org/10.1021/jacsau.4c00033

Author Contributions

Y.W. and H.Y. conceived the project. T.M. and F.Z. designed and trial-produced CGM. T.M., F.Z., Y.H., and Y.W. assembled the bioelectronic system. T.M. and G.Y. conducted the animal tests. T.M., G.Y., and L.L. processed and organized the data. Y.S. and S.D. helped characterize with constructive discussions. T.M., Y.W., S.D., and H.P. composed the paper. All authors read and agreed on the manuscript. CRediT: **Tiantian Man** data curation, writing-original draft; **Guiling Yu** investigation, methodology; **Fulin Zhu** data curation, investigation; **Yaqi Huang** investigation, methodology; **Yueyu Wang** investigation, software; **Yan Su** resources, supervision; **Sheng-Yuan Deng** conceptualization, project administration, writing-review & editing; **Hao Pei** conceptualization, writing-review & editing; **Li Li** conceptualization, supervision; **Haifeng Ye** conceptualization, resources, supervision; **Ying Wan** funding acquisition, project administration, supervision, writing-review & editing.

Notes

The authors declare no competing financial interest.

https://doi.org/10.1021/jacsau.4c00033
JACS Au 2024, 4, 1500−1508

■ ACKNOWLEDGMENTS

This project was financially supported by National Natural Science Foundation of China (Grant nos. 22204077, 22374076), China Postdoctoral Science Foundation (2021M701722), Natural Science Foundation of Jiangsu Province (BK20231455), Fundamental Research Funds for the Central Universities (30921013112, 30922010501), and Postgraduate Research & Practice Innovation Program of Jiangsu Province (KYCX23_0445).

■ REFERENCES

(1) Zhang, J.; Li, Y.; Li, H.; Zhu, B.; Wang, L.; Guo, B.; Xiang, L.; Dong, J.; Liu, M.; Xiang, G. GDF11 Improves Angiogenic Function of EPCs in Diabetic Limb Ischemia. *Diabetes* **2018**, *67*, 2084−2095.
(2) Saeedi, P.; Petersohn, I.; Salpea, P.; Malanda, B.; Karuranga, S.; Unwin, N.; Colagiuri, S.; Guariguata, L.; Motala, A. A.; Ogurtsova, K.; Shaw, J. E.; Bright, D.; Williams, R. Global and regional diabetes prevalence estimates for 2019 and projections for 2030 and 2045: Results from the International Diabetes Federation Diabetes Atlas, 9th edition. *Diabetes Res. Clin. Pract.* **2019**, *157*, 107843.
(3) Silver, B.; Ramaiya, K.; Andrew, S. B.; Fredrick, O.; Bajaj, S.; Kalra, S.; Charlotte, B. M.; Claudine, K.; Makhoba, A. EADSG Guidelines: Insulin Therapy in Diabetes. *Diabetes Ther.* **2018**, *9*, 449−492.
(4) Shao, J.; Xue, S.; Yu, G.; Yu, Y.; Yang, X.; Bai, Y.; Zhu, S.; Yang, L.; Yin, J.; Wang, Y.; Liao, S.; Guo, S.; Xie, M.; Fussenegger, M.; Ye, H. Smartphone-controlled optogenetically engineered cells enable semiautomatic glucose homeostasis in diabetic mice. *Sci. Transl. Med.* **2017**, *9* (387), No. eaal2298.
(5) Lee, H. J.; Choi, T. K.; Lee, Y. B.; Cho, H. R.; Ghaffari, R.; Wang, L.; Choi, H. J.; Chung, T. D.; Lu, N. S.; Hyeon, T. H.; Choi, S. H.; Kim, D.-H. A Graphene-Based Electrochemical Device with Thermoresponsive Microneedles for Diabetes Monitoring and Therapy. *Nat. Nanotechnol.* **2016**, *11* (6), 566−572.
(6) Yu, J.; Zhang, Y.; Ye, Y.; DiSanto, R.; Sun, W.; Ranson, D.; Ligler, F. S.; Buse, J. B.; Gu, Z. Microneedle-Array Patches Loaded with Hypoxia-Sensitive Vesicles Provide Fast Glucose-Responsive Insulin Delivery. *Proc. Natl. Acad. Sci. U. S. A.* **2015**, *112*, 8260−8265.
(7) Yu, J.; Wang, J.; Zhang, Y.; Chen, G.; Mao, W.; Ye, Y.; Kahkoska, A. R.; Buse, J. B.; Langer, R.; Gu, Z. Glucose-Responsive Insulin Patch for the Regulation of Blood Glucose in Mice and Minipigs. *Nat. Biomed. Eng.* **2020**, *4*, 499−506.
(8) Zhang, Y.; Wu, M.; Tan, D.; Liu, Q.; Xia, R.; Chen, M.; Liu, Y.; Xue, L.; Lei, Y. A Dissolving and Glucose-Responsive Insulin-Releasing Microneedle Patch for Type 1 Diabetes Therapy. *J. Mater. Chem. B* **2021**, *9*, 648−657.
(9) Tauschmann, M.; Hovorka, R. Technology in the Management of Type 1 Diabetes Mellitus-Current Status and Future Prospects. *Nat. Rev. Endocrinol.* **2018**, *14*, 464−475.
(10) Lee, H. J.; Song, C. Y.; Hong, Y. S.; Kim, M. S.; Cho, H. R.; Kang, T. G.; Shin, K. G.; Choi, S. H.; Hyeon, T. W.; Kim, D. H. Wearable/Disposable Sweat-Based Glucose Monitoring Device with Multistage Transdermal Drug Delivery Module. *Sci. Adv.* **2017**, *3*, No. e1601314.
(11) Wang, J.; Wang, Z.; Yu, J.; Kahkoska, A. R.; Buse, J. B.; Gu, Z. Glucose-Responsive Insulin and Delivery Systems: Innovation and Translation. *Adv. Mater* **2020**, *32* (13), 1902004.
(12) Zhao, J.; Xu, G.; Yao, X.; Zhou, H.; Lyu, B.; Pei, S.; Wen, P. Microneedle-Based Insulin Transdermal Delivery System: Current Status and Translation Challenges. *Drug Delivery Transl. Res.* **2022**, *12*, 2403−2427.
(13) Keum, D. H.; Jung, H. S.; Wang, T.; Shin, M. H.; Kim, Y. E.; Kim, K. H.; Ahn, G. O.; Hahn, S. K. Microneedle Biosensor for Real-Time Electrical Detection of Nitric Oxide for In Situ Cancer Diagnosis during Endomicroscopy. *Adv. Healthc. Mater.* **2015**, *4*, 1153−1158.
(14) Samant, P. P.; Prausnitz, M. R. Mechanisms of Sampling Interstitial Fluid from Skin Using a Microneedle Patch. *Proc. Natl. Acad. Sci. U. S. A.* **2018**, *115*, 4583−4588.
(15) Shao, J.; Wang, M.; Yu, G.; Zhu, S. Synthetic Far-Red Light-Mediated CRISPR-dCas9 Device for Inducing Functional Neuronal Differentiation. *Proc. Natl. Acad. Sci. U. S. A.* **2018**, *115* (29), No. E6722.
(16) Zhou, Y.; Kong, D.; Wang, X.; Yu, G.; Wu, X.; Guan, N.; Weber, W.; Ye, H. A Small and Highly Sensitive Red/Far-Red Optogenetic Switch for Applications in Mammals. *Nat. Biotechnol.* **2022**, *40*, 262−272.
(17) Guo, X.; Gorodetsky, A. A.; Hone, J.; Barton, J. K.; Nuckolls, C. Conductivity of a Single DNA Duplex Bridging a Carbon Nanotube Gap. *Nat. Nanotechnol.* **2008**, *3*, 163−167.
(18) Sun, L.; Gao, Y.; Xu, Y.; Chao, J.; Liu, H.; Wang, L.; Li, D.; Fan, C. Real-Time Imaging of Single-Molecule Enzyme Cascade Using a DNA Origami Raft. *J. Am. Chem. Soc.* **2017**, *139*, 17525−17532.
(19) Clever, G. H.; Shionoya, M. Metal-Base Pairing in DNA. *Coord. Chem. Rev.* **2010**, *254*, 2391−2402.
(20) Liu, H.; Shen, F.; Haruehanroengra, P.; Yao, Q.; Cheng, Y.; Chen, Y.; Yang, C.; Zhang, J.; Wu, B.; Luo, Q.; Cui, R.; Li, J.; Ma, J. A DNA Structure Containing AgI-Mediated G: G and C: C Base Pairs. *Angew. Chem., Int. Ed. Engl.* **2017**, *56*, 9430−9434.
(21) Tang, Q.; Plank, T. N.; Zhu, T.; Yu, H.; Ge, Z.; Li, Q.; Li, L.; Davis, J. T.; Pei, H. Self-Assembly of Metallo-Nucleoside Hydrogels for Injectable Materials that Promote Wound Closure. *ACS Appl. Mater. Interfaces* **2019**, *11*, 19743−19750.
(22) Ono, A.; Cao, S.; Togashi, H.; Tashiro, M.; Fujimoto, T.; Machinami, T.; Oda, S.; Miyake, Y.; Okamoto, I.; Tanaka, Y. Specific Interactions between Silver (I) Ions and Cytosine-Cytosine Pairs in DNA Duplexes. *Chem. Commun.* **2008**, *39*, 4825−4827.
(23) Pei, H.; Sha, R.; Wang, X.; Zheng, M.; Fan, C.; Canary, J. W.; Seeman, N. C. Organizing End-Site-Specific SWCNTs in Specific Loci Using DNA. *J. Am. Chem. Soc.* **2019**, *141*, 11923−11928.
(24) Ahern, A. M.; Garrell, R. L. In Situ Photoreduced Silver Nitrate as a Substrate for Surface-Enhanced Raman Spectroscopy. *Anal. Chem.* **1987**, *59*, 2813−2816.
(25) Maillard, M.; Huang, P.; Brus, L. Silver Nanodisk Growth by Surface Plasmon Enhanced Photoreduction of Adsorbed [Ag^+]. *Nano Lett.* **2003**, *3*, 1611−1615.
(26) Alekseev, V.; Semenov, A.; Pakhomov, P. Complexation of Ag^+ Ions with L-Cysteine. *Russ. J. Inorg. Chem.* **2012**, *57*, 1041−1044.
(27) Randazzo, R.; Mauro, A. D.; D'Urso, A.; Messina, G. C.; Compagnini, G.; Villari, V.; Micali, N.; Purrello, R.; Fragalà, M. E. Hierarchical Effect behind the Supramolecular Chirality of Silver(I)−Cysteine Coordination Polymers. *J. Phys. Chem. B* **2015**, *119* (14), 4898−4904.
(28) Hu, Y.; Rehnlund, D.; Klein, E.; Gescher, J.; Niemeyer, C. M. Cultivation of Exoelectrogenic Bacteria in Conductive DNA Nanocomposite Hydrogels Yields a Programmable Biohybrid Materials System. *ACS Appl. Mater. Interfaces* **2020**, *12*, 14806−14813.
(29) Dvir, T.; Timko, B. P.; Brigham, M. D.; Naik, S. R.; Karajanagi, S. S.; Levy, O.; Jin, H.; Parker, K. K.; Langer, R.; Kohane, D. S. Nanowired Three-Dimensional Cardiac Patches. *Nat. Nanotechnol.* **2011**, *6*, 720−725.
(30) Shin, S. R.; Jung, S. M.; Zalabany, M.; Kim, K. Y.; Zorlutuna, P.; Kim, S. B.; Nikkhah, M.; Khabiry, M.; Azize, M.; Kong, J.; Wan, K. T.; Palacios, T.; Dokmeci, M. R.; Bae, H.; Tang, X.; Khademhosseini, A. Carbon-Nanotube-Embedded Hydrogel Sheets for Engineering Cardiac Constructs and Bioactuators. *ACS Nano* **2013**, *7*, 2369−2380.
(31) Ohm, Y.; Pan, C.; Ford, M. J.; Huang, X.; Liao, J.; Majidi, C. An Electrically Conductive Silver-Polyacrylamide-Alginate Hydrogel Composite for Soft Electronics. *Nat. Electron.* **2021**, *4*, 185−192.
(32) Liang, B.; Qin, Z.; Zhao, J.; Zhang, Y.; Zhou, Z.; Lu, Y. Controlled Synthesis, Core-Shell Structures and Electrochemical Properties of Polyaniline/Polypyrrole Composite Nanofibers. *J. Mater. Chem. A* **2014**, *2*, 2129−2135.
(33) Warren, H.; Gately, R. D.; O'Brien, P.; Gorkin III, R.; In Het Panhuis, M. Electrical Conductivity, Impedance, and Percolation

https://doi.org/10.1021/jacsau.4c00033
JACS Au 2024, 4, 1500−1508

Behavior of Carbon nanofiber and Carbon Nanotube Containing Gellan Gum Hydrogels. *J. Polym. Sci., Part B: Polym. Phys.* **2014**, *52*, 864−871.
(34) Ghosh, S.; Inganäs, O. Electrochemical Characterization of Poly (3,4-ethylene dioxythiophene) Based Conducting Hydrogel Networks. *J. Electrochem. Soc.* **2000**, *147*, 1872.
(35) Dai, T.; Qing, X.; Lu, Y.; Xia, Y. Conducting Hydrogels with Enhanced Mechanical Strength. *Polymer* **2009**, *50*, 5236−5241.
(36) Zhong, R.; Tang, Q.; Wang, S.; Zhang, H.; Zhang, F.; Xiao, M.; Man, T.; Qu, X.; Li, L.; Zhang, W.; Pei, H. Self-Assembly of Enzyme-Like Nanofibrous G-Molecular Hydrogel for Printed Flexible Electrochemical Sensors. *Adv. Mater.* **2018**, *30* (12), 1706887.
(37) Sarker, M.; Chen, X. B. Modeling the Flow Behavior and Flow Rate of Medium Viscosity Alginate for Scaffold Fabrication with a Three-Dimensional Bioplotter. *J. Manuf. Sci. Eng.* **2017**, *139*, 081002.
(38) Sweeney, M.; Campbell, L. L.; Hanson, J.; Pantoya, M. L.; Christopher, G. F. Characterizing the Feasibility of Processing Wet Granular Materials to Improve Rheology for 3D Printing. *J. Mater. Sci.* **2017**, *52*, 13040−13053.
(39) Lee, S. C.; Gillispie, G.; Prim, P.; Lee, S. J. Physical and Chemical Factors Influencing the Printability of Hydrogel-Based Extrusion Bioinks. *Chem. Rev.* **2020**, *120*, 10834−10886.
(40) Xie, C.; Wang, X.; He, H.; Ding, Y.; Lu, X. Mussel-Inspired Hydrogels for Self-Adhesive Bioelectronics. *Adv. Funct. Mater.* **2020**, *30* (25), 1909954.
(41) Mehrali, M.; Thakur, A.; Pennisi, C. P.; Talebian, S.; Arpanaei, A.; Nikkhah, M.; Dolatshahi-Pirouz, A. Nanoreinforced Hydrogels for Tissue Engineering: Biomaterials That Are Compatible with Load-Bearing and Electroactive Tissues. *Adv. Mater.* **2017**, *29* (8), 1603612.
(42) Tringides, C. M.; Vachicouras, N.; Lázaro, I. D.; Wang, H.; Trouillet, A.; Seo, B. R.; Elosegui-Artola, A.; Fallegger, F.; Shin, Y. Y.; Casiraghi, C.; Kostarelos, K.; Lacour, S. P.; Mooney, D. J. Viscoelastic Surface Electrode Arrays to Interface with Viscoelastic Tissues. *Nat. Nanotechnol.* **2021**, *16* (9), 1019−1029.
(43) Martanto, W.; Davis, S. P.; Holiday, N. R.; Wang, J.; Gill, H. S.; Prausnitz, M. R. Transdermal Delivery of Insulin Using Microneedles in Vivo. *Pharm. Res.* **2004**, *21*, 947−952.
(44) Sarabi, M. R.; Ahmadpour, A.; Yetisen, A. K.; Tasoglu, S. Finger-Actuated Microneedle Array for Sampling Body Fluids. *Appl. Sci.* **2021**, *11*, 5329−5345.
(45) Keller, L. A.; Merkel, O.; Popp, A. Intranasal Drug Delivery: Opportunities and Toxicologic Challenges during Drug Development. Drug Deliv. *Drug Delivery Transl. Res.* **2022**, *12*, 735−757.
(46) Bailey, T.; Bode, B. W.; Christiansen, M. P.; Klaff, L. J.; Alva, S. The Performance and Usability of a Factory-Calibrated Flash Glucose Monitoring System. *Diabetes Technol. Ther.* **2015**, *17*, 787−794.
(47) Advani, A. Positioning Time in Range in Diabetes Management. *Diabetologia* **2020**, *63*, 242−252.
(48) Trevitt, S.; Simpson, S.; Wood, A. Artificial Pancreas Device Systems for the Closed-Loop Control of Type 1 Diabetes: What Systems Are in Development? *J. Diabetes Sci. Technol.* **2016**, *10*, 714−723.
(49) Gao, M.; Krissanaprasit, A.; Miles, A.; Hsiao, L. C.; LaBean, T. H. Mechanical and Electrical Properties of DNA Hydrogel-Based Composites Containing Self-Assembled Three-Dimensional Nanocircuits. *Appl. Sci.* **2021**, *11*, 2245−2259.
(50) Li, F.; Tang, J.; Geng, J.; Luo, D.; Yang, D. Polymeric DNA Hydrogel: Design, Synthesis and Applications. *Prog. Polym. Sci.* **2019**, *98*, 101163.
(51) Yao, G.; Yin, C.; Wang, Q.; Zhang, T.; Chen, S.; Lu, C.; Zhao, K.; Xu, W.; Pan, T.; Gao, M.; Lin, Y. Flexible Bioelectronics for Physiological Signals Sensing and Disease Treatment. *J. Materiomics* **2020**, *6*, 397−413.
(52) Song, J.; Zhang, Y.; Chan, S. Y.; Du, Z.; Yan, Y.; Wang, T.; Li, P.; Huang, W. Hydrogel-Based Flexible Materials for Diabetes Diagnosis, Treatment, and Management. *NPJ. Flex. Electron.* **2021**, *5*, 26.
(53) Choi, Y. S.; Yin, R. T.; Pfenniger, A.; Koo, J. H.; Avila, R.; Lee, K. B.; Chen, S. W.; Lee, G. B.; Li, G.; Qiao, Y.; et al.et al Fully Implantable and Bioresorbable Cardiac Pacemakers without Leads or Batteries. *Nat. Biotechnol.* **2021**, *39* (10), 1228−1238.
(54) Tehrani, F.; Teymourian, H.; Wuerstle, B.; Kavner, J.; Patel, R.; Furmidge, A.; Aghavali, P. P.; Wang, H.; Brown, C.; Zhang, F.; et al.etal An Integrated Wearable Microneedle Array for the Continuous Monitoring of Multiple Biomarkers in Interstitial Fluid. *Nat. Biomed. Eng.* **2022**, *6* (11), 1214−1224.
(55) Zhao, G.; Liu, G. Electrochemical Deposition of Gold Nanoparticles on Reduced Graphene Oxide by Fast Scan Cyclic Voltammetry for the Sensitive Determination of As(III). *Nanomaterials* **2019**, *9*, 41−53.
(56) Xiao, M.; Zou, K.; Li, L.; Wang, L.; Tian, Y.; Fan, C.; Pei, H. Stochastic DNA Walkers in Droplets for Super-Multiplexed Bacterial Phenotype Detection. *Angew. Chem., Int. Ed.* **2019**, *58*, 15448−15454.
(57) Liu, L.; Liu, Y.; Zhang, Y.; Yuan, R.; Wang, H. K-Doped Graphitic Carbon Nitride with Obvious Less Electrode Passivation for Highly Stable Electrochemiluminescence and its Sensitive Sensing Analysis of MicroRNA. *Anal. Chem.* **2022**, *94*, 7191−7199.
(58) Kolluru, C.; Williams, M.; Chae, J.; Prausnitz, M. R. Recruitment and Collection of Dermal Interstitial Fluid using a Microneedle Patch. *Adv. Healthcare Mater.* **2019**, *8* (3), 1801262.

https://doi.org/10.1021/jacsau.4c00033
JACS Au 2024, 4, 1500−1508